Condensation-driven hydration of porous paperboard: coupled heat–mass transport, pore flooding, and climatic sensitivity

International Journal of Thermal Sciences 230 (2026) 111188

Contents lists available at ScienceDirect

International Journal of Thermal Sciences

journal homepage: www.elsevier.com/locate/ijts

Condensation-driven hydration of porous paperboard: coupled heat–mass transport, pore flooding, and climatic sensitivity

Raffaella De Piano [a], Diego Caccavo [a,b], Antonia Calabrese [a], Anna Angela Barba [b,c], Anette Larsson [d], Gaetano Lamberti [a,b,*]

[a] Dipartimento di Ingegneria Industriale, Università degli Studi di Salerno, Via Giovanni Paolo II, Fisciano, SA, I-84084, Italy
[b] EST Srl, Via Circumvallazione 39, Avellino, I-83100, Italy
[c] Dipartimento di Farmacia, Università degli Studi di Salerno, Via Giovanni Paolo II, Fisciano, SA, I-84084, Italy
[d] FibRe – Centre for Lignocellulose-based Thermoplastics, Chemistry and Chemical Engineering, Chalmers University of Technology, Gothenburg, 412 96, Sweden

ARTICLE INFO

Keywords:
Paperboard cups
Water adsorption
Condensation
Porous media
Heat and mass transfer

ABSTRACT

The hydration of paperboard walls in cups filled with cold beverages arises from coupled heat and mass transfer phenomena. While classical studies describe moisture uptake only in the hygroscopic range, the behavior under condensation remains largely unexplored. In this work, we extend the water–paper adsorption isotherm into the supersaturated regime, perform dynamic hydration experiments on cups exposed to iced water, and develop a mechanistic model to capture the observed kinetics.

Experiments reveal that once supersaturation occurs (relative humidity larger than one), water content on a dry basis rises sharply, suggesting liquid saturation levels approaching pore-filling conditions. Time-resolved measurements show a two-stage process: an initial rapid uptake linked to condensation and filling of accessible pores, followed by a slower diffusion- and capillary-controlled regime. The coupled model, which incorporates vapor diffusion, liquid imbibition, and heat transfer, was calibrated using the effective water diffusivity as a single fitting parameter and thus the model reproduced the experimental data with good accuracy. Applied as a predictive tool, the model anticipates cup behavior under diverse climates: low hydration in dry winters, moderate in dry summers, and critical uptake in humid summers.

This combined experimental–modeling approach provides a robust framework to predict condensation-driven water uptake and supports the design of sustainable paper-based packaging.

1. Introduction

1.1. Problem statement

The industrial production of disposable cups for both hot beverages is predominantly based on coupled bi-layer systems, typically consisting of a paperboard substrate coated with a thin polymeric film, most commonly polyethylene (PE) or biodegradable alternatives. This structural solution has emerged as a compromise between mechanical strength, printability, liquid barrier performance, as well as recyclability and sustainability. While the paperboard layer provides rigidity, stiffness, and formability, the plastic layer ensures liquid tightness and heat sealability, thus preventing leakage and structural degradation during use. For cold beverages a three-layers design is becoming the new industrial standard, in which PE-paperboard-PE are layered in order to provide structure and strength, and at same time prevent water absorption as well water condensation at the external surface. However, the bilayer design is still in use also for cold drinks, even it is not the optimum in this last case.

However, despite its widespread adoption and apparent simplicity, the performance of the bi-layer system is far from trivial, as it results from the interaction of complex thermo-hygrometric processes that occur in real service conditions. Indeed, these laminates operate under complex thermo-hygrometric loads, where atmospheric moisture and temperature gradients interact in time-dependent ways, influencing durability and service behavior [1–3].

In particular, the humidification of the paperboard layer, primarily driven by the absorption of atmospheric water vapor (thinking of a bi-

* Corresponding author. comment_hash{commentForInsertingAff}Dipartimento di Ingegneria Industriale, Università degli Studi di Salerno, Via Giovanni Paolo II, I-84084, Fisciano, (SA), Italy.
E-mail address: glamberti@unisa.it (G. Lamberti).

https://doi.org/10.1016/j.ijthermalsci.2026.111188
Received 1 March 2026; Received in revised form 21 June 2026; Accepted 11 July 2026
Available online 15 July 2026

layer design), plays a crucial role in determining the durability and functional stability of cups. Paper, as a hygroscopic material, undergoes dimensional changes, variations in stiffness, and alterations of its barrier properties upon moisture uptake, which may compromise consumer experience and product reliability [4].

From an industrial perspective, the scale is non-trivial: recent market assessments place the global paper-cup segment around USD 8.7–14.3 billion in 2024, with forecasts to ~USD 11.8–19.7 billion by 2033–2034 [5–7], while adjacent "disposable cups" estimates (covering paper and plastic) report ~ USD 17.4 billion in 2024 [8]. It should be noted that market estimates vary by scope (paper-only vs. "disposable cups") and methodology; the ranges reported above reflect this spread. Anyway, these figures underscore both the economic relevance of performance-reliable, humidity-tolerant paper–polymer laminates and the value of predictive modeling to guide materials selection, laminate design and storage/use protocols across hot and cold beverage applications.

1.2. State of the art

From a physical point of view, the coupled heat and mass transfer phenomena in the paper-cup bi-layer structures represent a nontrivial multiphase problem. The moisture transport is governed by diffusion through porous cellulose fibers, sorption kinetics at the fiber–air interface, and possible redistribution along the fiber network, while the polymeric layer limits but does not completely prevent water vapor penetration at the exposed rim and interfaces. Simultaneously, the presence of hot or cold liquids inside the cup establishes a temperature gradient across the wall, which modifies the local vapor pressure and enhances or suppresses condensation phenomena.

Thermal gradients induced by hot (~60-90 °C) or cold (~0-5 °C) beverages complicate the coupled heat and mass transfer processes: in hot-fill scenarios, the thermal stress on the polymer coating can induce micro-defects or accelerate softening, while the paperboard substrate undergoes differential expansion due to non-uniform humidification that, in turn, can produce differential hygro-expansion, out-of-plane instabilities and local damage [9], [10]; in cold-fill use, external condensation contributes to moisture uptake from outside to inside, affecting haptic properties and mechanical integrity ([11], [12]).

Thus, the overall performance of polymer coated-paperboard cups is controlled by a coupled thermo-hygro-mechanical process, where heat conduction, phase change, and moisture diffusion interact within a heterogeneous layered structure.

While previous studies have primarily focused on moisture sorption under sub-saturated conditions or on the barrier properties of paper-based laminates, the present work specifically addresses condensation-driven hydration under supersaturated conditions through a combined experimental and modeling approach.

Given the industrial scale of paper cup production and usage – estimated at hundreds of billions of units annually (furthermore, it is still a well-established industry practice to use two-side polymer coated paperboard in the production of cold-beverage cups) – the capacity to predict and control these phenomena is of paramount relevance. On the one hand, understanding the humidification dynamics is essential for optimizing material formulations, such as the selection of fiber treatments, sizing agents, and alternative biopolymers to reduce moisture sensitivity. On the other hand, it supports the design of improved industrial storage and distribution strategies, mitigating quality loss and waste. It is noticeable that, in the ambition to reduce the amount of polymer coating, it is also of interest to understand if the outer polymer coating can be replaced with another barrier structure, and, if so, what the barrier properties of such barrier structure need to be in normal service life.

Mathematical modeling emerges as a powerful tool to address these challenges, offering a rational framework for quantifying heat and mass transfer in paper–polymer systems under realistic boundary conditions. Advanced models based on coupled partial differential equations (heat and mass balances) can describe sorption isotherms, moisture diffusivity, temperature profiles, and their time evolution within the bi-layer structure. When validated against experimental data, such models enable predictive simulations that can guide industrial practice, from process design to end-use performance assessment. Moreover, modeling is indispensable for comparative evaluation of traditional petroleum-based coatings versus novel biodegradable alternatives, allowing industry to accelerate the transition toward sustainable packaging without compromising reliability. For these reasons, the scientific and industrial communities increasingly recognize that a systematic, model-based approach to humidification phenomena in coupled plastic–paper structures is a key step toward engineering next-generation food contact materials with optimized performance, environmental compatibility, and consumer safety.

Mathematical modeling provides a rigorous framework to quantify these coupled heat-and-mass phenomena [13,14]. Continuum transport models incorporating Fickian diffusion, nonlinear sorption isotherms, and transient energy balance equations have proven effective, particularly when extended to thermo-hygro-mechanical models that predict bend, warping, or delamination from hygroscopic strain and stiffness changes [9], [4,10,15]. In cold-beverage scenarios, models capture condensation-driven moisture ingress via surface mass-transfer boundary conditions, with liquid uptake modeled through capillary imbibition or diffusion into the fiber network. Hybrid models have emerged, coupling finite element analyses of layered structures with experimentally derived sorption isotherms, diffusivity data, and coating permeability values ([11], [3]).

Complementary to modeling, experimental techniques are indispensable to parameterize and validate these descriptions. Gravimetric sorption analysis, typically performed with dynamic vapor sorption (DVS) instruments, provides equilibrium sorption isotherms and diffusivity values over a wide range of relative humidities, essential for populating Fickian or dual-mode transport models [4]. Thermal conductivity and heat capacity of paper–polymer laminates have been measured with transient plane source or differential scanning calorimetry methods to provide input for heat-transfer models [16]. Water vapor transmission rate (WVTR) tests, standardized in packaging research, are used to quantify barrier properties of the polymer coating and to assess the additional effect of humidified paper substrate. For cold-beverage conditions, controlled condensation chambers allow simultaneous measurement of external condensation rate and liquid uptake by paper cups, enabling correlations with tactile or mechanical degradation. In hot-beverage applications, immersion and fill-tests at elevated temperatures are conducted to observe delamination, coating softening, or leaching phenomena; analytical methods such as FTIR or SEM imaging are applied to detect coating micro-defects or migration of polymer residues [12]. Hygro-mechanical testing under controlled humidity (e.g., tensile, bending, or compression tests in climate chambers) has also been employed to characterize stiffness reduction upon humidification ([11]). Increasingly, full-scale tests replicate realistic service: cups are filled with hot coffee or iced soda and monitored for dimensional stability, leakage, and surface feel, while digital image correlation techniques quantify strain and deformation.

Importantly, the integration of modeling and experimentation creates a feedback loop: experimental sorption and transport data serve as input parameters and validation points for mathematical models, while modeling guides the design of targeted experiments under specific thermal and humidity conditions. Recent studies have further highlighted the role of biodegradable coatings (PLA, PHB, starch-based) in altering these coupled processes, requiring both modified models for water-vapor permeability and specialized experimental protocols for bio-based laminates [1,2,17]. For industry, this combined methodology enables not only the prediction of performance under diverse conditions – hot beverages in winter, iced sodas in humid summer environments – but also the accelerated evaluation of next-generation sustainable cup

designs, reducing reliance on empirical trial-and-error. Thus, the state-of-the-art in paper cup research rests on the synergy between physically based thermo-hygro-mechanical modeling and increasingly sophisticated experimental techniques, both essential to ensuring product reliability and supporting the transition toward environmentally responsible disposable packaging.

1.3. Aims of this work

While a wide range of studies exist on hygroscopic behavior of paper and barrier performance of coatings (Table 1), there remains a lack of integrated kinetic–thermodynamic models that simultaneously describe condensation, sorption, and water up-take under realistic beverage service conditions and different environmental conditions. This gap is particularly relevant for cold sodas and iced beverages, where environmental factors (temperature, humidity, airflow) strongly modulate external condensation and subsequent paper weakening.

The present work addresses this need by: (i) experimentally extending the water–paper sorption relationship into the supersaturated regime relevant to condensation phenomena; (ii) developing a coupled heat- and mass-transfer model capable of describing condensation-driven hydration in porous paperboard; (iii) validating the model against controlled hydration experiments; and (iv) applying the validated model as a predictive tool to investigate the influence of different environmental conditions on cup hydration.

A distinctive feature of the present work is the integration of controlled hydration experiments with a mechanistic heat- and mass-transfer model, allowing experimental observations and theoretical predictions to be interpreted within a unified framework.

It should be noted that, to the purpose of this work, only two-layers paper cups have been considered, both because they are still used for cold beverages in the market (even if the market is shifting toward the best performing three layers design) and in order to establish the modeling framework which could be enlarged in the future to analyze the three-layers paper cups.

2. Materials and methods

2.1. Materials

The experimental section of this work has required just the use of cold tap water plus ice cubes, and paper cups. Two sizes of PE coated paper cups have been used, and their characteristics are summarized in Table 2. The paper layer thickness was determined by direct measurement using a caliper after wall cut and delamination (manually remotion the PE layer).

2.2. Methods

2.2.1. Water content

The water contents of paper samples were measured by a thermobalance (Precisa XM 60 Series 330 XM), both for cup characterization and for dynamic experiments.

Before gravimetric determination, the external surface of each sample was gently blotted with absorbent paper in order to remove visible surface condensate. Consequently, the measured water uptake refers to water retained within or strongly associated with the paperboard structure rather than to free liquid droplets remaining on the outer surface.

2.2.2. Bulk density

Bulk density was calculated as the ratio between the dry mass and the sample volume. The volume was calculated from direct geometrical measurements of the size of regular pieces of paper layer. The dry mass

Table 2
Characteristics of tested paper cups.

	Size “A” (small)	Size “B” (large)
Volume	75 mL	185 mL
Height	5 cm	11 cm
Material(s)	Paper + PE	Paper + PE
Paper layer thickness	0.13 mm	0.13 mm

Table 1
Summary of studies on paper cup/paperboard laminate behavior under different thermo-hygrometric conditions.

Paper/Paper-cup	Conditions Studied	Main Results	Beverage Type/Application	Reference
Multi-ply paperboard	Hygro-expansion and out-of-plane deformation under variable RH	Demonstrated strong correlation between ambient RH and paperboard instability; demonstrated role of fiber orientation in dimensional changes.	General paperboard packaging; implications for both hot (swelling at high RH near hot liquids) and cold (condensation-related expansion).	[9]
Paper and books (cellulose-based)	Sorption kinetics, isotherms, hysteresis across RH cycles	Provided kinetic sorption models and evidence of delayed equilibrium; proposed coupled sorption–diffusion framework applicable to packaging.	Both hot and cold beverages; informs fundamental modeling of moisture uptake in cups.	[4]
Corrugated board (multi-layer)	Coupled humidity and temperature loads; FEM-based hygro-mechanical modeling	Validated numerical models against experiments showed stiffness and strength degradation under humid, warm conditions.	Mainly hot beverages (temperature-driven weakening); applicable to warm/humid storage of cups.	[22]
Paperboard with different coatings	Storage under varying humidity, contact with food	Reported significant loss in barrier function and stiffness under humid storage; biodegradable coatings more sensitive than PE.	Both hot and cold beverages; highlight storage risks before filling.	[3]
Biodegradable coatings on paper	Barrier tests, water vapor transmission rate (WVTR), thermal exposure	Identified critical limits in barrier performance at high humidity and elevated temperature; stressed need for improved coating formulations.	Hot beverages (thermal stress and coating softening).	[2]
Bio-based coatings for paper	WVTR, oxygen barrier, food packaging applications	Demonstrated reduction in water vapor permeability compared to uncoated paper; emphasized role of multilayer coatings.	Both hot and cold; key to improving cup performance under condensation and high RH.	[1]
Paper and polymer seals	Thermal conductivity and heat capacity under hot/cold exposure	Measured thermo-physical properties of coated paper; showed coating strongly influences heat transfer relevant to hot/cold beverages.	Both hot (thermal insulation) and cold (condensation management).	[15]
Commercial paper cups	Hot and cold fill; release of microplastics and leachables	Detected particle release and catalase activity inhibition; release accelerated at higher temperatures and prolonged exposure.	Both hot (coffee/tea) and cold sodas; safety perspective.	[11]
Paperboard packaging	Hygro-mechanical deformation and packaging performance	Detailed failure mechanisms (buckling, softening) under humid storage; integrated DIC-based deformation analysis with FEM.	Mainly cold sodas and humid environments (condensation-driven weakening).	[10]

was measured after drying of the sample by thermobalance.

3. Modeling

3.1. Expressions of water concentration in solid samples

In a sample of fibrous paper containing a certain amount of water, the water concentration could be expressed as the *water mass fraction (on wet basis)* as:

$$\omega_A [=] \frac{\mathrm{kg_{water}}}{\mathrm{kg_{s,wet}}} = \frac{\mathrm{kg_{water}}}{\mathrm{kg_{s,dry}} + \mathrm{kg_{water}}} \tag{1}$$

In equation (1) kg_{water} is the mass of water in the sample, $kg_{s,dry}$ is the mass of the dry solids in the sample, and $kg_{s,wet}$ is the mass of dry solids plus water, or wet solids, in the sample. The masses of gases (air and water vapor) were neglected.

An alternative expression is the *water mass fraction (on dry basis)*, which is given by:

$$\Omega_A [=] \frac{\mathrm{kg_{water}}}{\mathrm{kg_{s,dry}}} \tag{2}$$

The two quantities connect to each other, starting from eq. (1):

$$\omega_A [=] \frac{\mathrm{kg_{water}}}{\mathrm{kg_{s,wet}}} = \frac{\mathrm{kg_{water}}}{\mathrm{kg_{s,dry}} + \mathrm{kg_{water}}} = \frac{\frac{\mathrm{kg_{water}}}{\mathrm{kg_{s,dry}}}}{1 + \frac{\mathrm{kg_{water}}}{\mathrm{kg_{s,dry}}}} [=] \frac{\Omega_A}{1 + \Omega_A} \tag{3}$$

The *wet density*, ρ_{wet}, of a humid paper sample, can be easily obtained from the water mass fraction (on wet basis), by:

$$\frac{1}{\rho_{wet}} = \frac{\omega_A}{\rho_{water}} + \frac{1 - \omega_A}{\rho_{bulk}} [=] \frac{\mathrm{m^3}}{\mathrm{kg_{s,wet}}} \tag{4}$$

In eq. (4) ρ_{water} is the density of pure liquid water and ρ_{bulk} is the bulk density of the sample.

The *water concentration, w*, in the sample is defined as:

$$w = \rho_{wet}\omega_A = \omega_A \left(\frac{\omega_A}{\rho_{water}} + \frac{1 - \omega_A}{\rho_{bulk}} \right)^{-1} [=] \frac{\mathrm{kg_{s,wet}}}{\mathrm{m^3}} \frac{\mathrm{kg_{water}}}{\mathrm{kg_{s,wet}}} = \frac{\mathrm{kg_{water}}}{\mathrm{m^3}} \tag{5}$$

3.2. Sorption equation

In porous paperboard, the humidity can be considered to be located mainly into the pores, since the diffusion in solid fibers is a really slow process [18]. In the pores, water can be present in liquid and in gas phases. Being ε_p the solid porosity (volume of pores over total sample volume) and s_l the liquid saturation (i.e. the fraction of the pore volume occupied by the liquid water), the water concentration can be expressed as the sum of the water contained in the pores in liquid state and in the gas state:

$$w = \varepsilon_p \left[\rho_l s_l + \rho_g \omega_v (1 - s_l) \right] \tag{6}$$

In eq. (6) ρ_l is the density of liquid phase (i.e. $\rho_l = \rho_{water}$) and ρ_g is the density of gas phase, made of air and water vapor, ω_v being the mass fraction of water in gas phase.

The *relative humidity (of the gas phase)* can be defined as:

$$\phi_w = \frac{P_v}{P_{sat}(T)} = \frac{c_v}{c_{sat}(T)} \tag{7}$$

Where P_v is the partial pressure of water vapor in gas phase, $P_{sat}(T)$ is the saturation pressure of water in air (which is function only of temperature), c_v is the (molar) concentration of water vapor in gas phase and $c_{sat}(T)$ is the corresponding saturation concentration. The relative humidity is related to the mass fraction of water in gas phase, since:

$$\omega_v = \frac{M_w c_v}{\rho_g} [=] \frac{\frac{\mathrm{kg_{water}}}{\mathrm{mol_{water}}} \frac{\mathrm{mol_{water}}}{\mathrm{m^3}}}{\frac{\mathrm{kg_{g,tot}}}{\mathrm{m^3}}} = \frac{\mathrm{kg_{water}}}{\mathrm{kg_{g,tot}}} [=] \frac{M_w \phi_w c_{sat}(T)}{\rho_g} \tag{8}$$

Where M_w is the water molar mass. Inserting eq. (8) into eq. (6) the relationship between relative humidity, ϕ_w, and water concentration in the sample, w, can be obtained. This relationship is the *sorption equation*, i.e. the *constitutive equation* which is the basis of mass transfer modeling.

$$w = w(\phi_w) \tag{9}$$

3.3. Transport equations

Two transport phenomena have been considered to describe what happens to the paper-cup in the transient starting immediately after pouring the cold soda into the cup: the mass and the heat transfer.

3.3.1. Mass transfer

The mass transfer is governed by the following balance equation:

$$\frac{\partial w(\phi_w)}{\partial t} = -\nabla \cdot \boldsymbol{g_w} - \nabla \cdot \boldsymbol{g_{lc}} \tag{10}$$

The accumulation term on the LHS is given by the time derivative of the water mass concentration, the two fluxes on the RHS are respectively the water vapor flux in the gas phase, $\boldsymbol{g_w}$, and the water capillary flux in the liquid phase, $\boldsymbol{g_{lc}}$. Both can be calculated using a pseudo-Fickian approach:

$$\boldsymbol{g_w} = D_{eff} \rho_g \nabla \omega_v \tag{11}$$

$$\boldsymbol{g_{lc}} = D_w \frac{\partial w(\phi_w)}{\partial \phi_w} \nabla \phi_w \tag{12}$$

In equations (11) and (12) all the variables have been already defined, but the effective diffusivity of vapor, D_{eff} (given by eq. (13)), and the moisture capillary diffusivity, D_w.

$$D_{eff} = \frac{\varepsilon_p (1 - s_l)}{\tau} D \tag{13}$$

In eq. (13) τ is the pore tortuosity and D is the diffusivity of water vapor in air. The pore tortuosity was estimated by the Bruggeman model, in which $\theta_g = \varepsilon_p (1 - s_l)$ is the volume fraction of the pores occupied by the gas phase:

$$\tau = \theta_g^{-5/2} \varepsilon_p^2 = \left[\varepsilon_p (1 - s_l) \right]^{-5/2} \varepsilon_p^2 \tag{14}$$

The diffusivity of water vapor in air was taken from literature [18], whereas the moisture capillary diffusivity, D_w was taken as the single fitting parameter of the model.

3.3.2. Heat transfer

The heat transfer is described by the equation of change for temperature:

$$(\rho C_P)_{eff} \frac{\partial T}{\partial t} = -\nabla \cdot \boldsymbol{q} + \mathrm{Q}_{parz} + Q_{evap} \tag{15}$$

The transient term on the LHS of equation (15) requires the definition of an 'effective' heat capacity, $(\rho C_P)_{eff}$, taking into account for heat capacity of the three different phases present (solid, liquid, and vapor). The three terms on the RHS of equation (15) describe respectively the heat transfer by conduction, $-\nabla \cdot \boldsymbol{q}$ ($\boldsymbol{q}$ being the conductive heat flux), by partial enthalpy transfer, Q_{parz}, and by evaporation, Q_{evap}.

$$(\rho C_P)_{eff} = (1 - \varepsilon_p) \rho_s C_{Ps} + \varepsilon_p \left[(1 - s_l) \rho_g C_{Pg} + s_l \rho_l C_{Pl} \right] \tag{16}$$

The 'effective' heat capacity, $(\rho C_P)_{eff}$, is evaluated by equation (16). The three terms on the RHS of equation (16) taken into account respectively for the heat capacity: 1) of the solid fraction (volumetric

fraction $(1-\varepsilon_p)$, density ρ_s, and specific heat C_{Ps}); 2) of the gaseous fraction (volumetric fraction $\varepsilon_p(1-s_l)$, density ρ_g and specific heat C_{Pg}); and 3) of the liquid fraction (volumetric fraction $\varepsilon_p s_l$, density ρ_l and specific heat C_{Pl}).

$$\boldsymbol{q} = -k_{eff}\nabla T \tag{17}$$

The conductive heat flux is a vector calculated by Fourier equation, in which the 'effective' conductivity, k_{eff}, can be estimated as:

$$k_{eff} = (1-\varepsilon_p)k_s + \varepsilon_p\left[(1-s_l)k_g + s_l k_l\right] \tag{18}$$

Similarly to equation (16), the three terms on the RHS of equation (19) taken into account respectively for the heat conductivity: 1) of the solid fraction (volumetric fraction $(1-\varepsilon_p)$, heat conductivity k_s); 2) of the gaseous fraction (volumetric fraction $\varepsilon_p(1-s_l)$, heat conductivity k_g); and 3) of the liquid fraction (volumetric fraction $\varepsilon_p s_l$, heat conductivity k_l).

To describe the partial enthalpy transfer both the effects of water vapor flux and of the capillary flux must be considered. All the terms on the RHS of equation (20) have been already defined and thus they are already known.

$$Q_{parz} = -\left[(C_{Pg}-C_{Pl})\boldsymbol{g_w} + C_{Pl}\boldsymbol{g_{lc}}\right]\cdot\nabla T \tag{21}$$

The heat flow rate due to evaporation is simply given (equation (22)) by the product between the latent heat of evaporation, ΔH_{evap}, and the mass flow rate of the evaporating water, G_{evap}.

$$Q_{evap} = \Delta H_{evap} G_{evap} \tag{23}$$

Last term to be evaluated is the mass flow rate of the evaporating water, G_{evap}, and this can be seen as the sum of the change of steam quantity over time in the volume fraction occupied by vapor ('real' evaporation) and the net flow rate due to the vapor flux, $\nabla\cdot\boldsymbol{g_w}$. Therefore, the desired term can be evaluated by the following equation (24).

$$G_{evap} = \frac{\partial}{\partial t}\left[\varepsilon_p(1-s_l)\rho_g\omega_v\right] + \nabla\cdot\boldsymbol{g_w} \tag{25}$$

3.3.3. Initial and boundary conditions

In order to solve the model, the two field variables: temperature, T, and relative humidity, ϕ_w (from which the water concentration, w, can be estimated by equation (9)) requires the initial values and properly defined boundary conditions.

As for the initial conditions, they have been taken as:

$$T = room\ temperature = T_{ext} \tag{26}$$

$$\phi_w = relative\ humidity\ in\ external\ (room)\ air = \phi_{w.ext} \tag{27}$$

The transport phenomena take place in a single direction, say it $x-axis$, therefore the problem is a 1D transient problem. The position $x=0$ is taken as the interface between the paperboard wall and the external air, the position $x=L$ is the interface between the paperboard wall and the inner iced water (neglecting the polymer coating). The thickness of the wall therefore has been taken equal to paperboard thickness, i.e. $L = 0.13\ mm$ (see Section 2.1).

At the interface between the paperboard wall and the external air ($x=0$) both the heat and mass fluxes can be estimated as convective fluxes:

$$-\boldsymbol{n}\cdot\boldsymbol{q} = h\left(T_{ext} - T|_{x=0}\right) \tag{28}$$

$$-\boldsymbol{n}\cdot\boldsymbol{g_w} = k_m M_w\left(c_{v,ext} - c_v|_{x=0}\right) \tag{29}$$

The interphase heat exchange coefficient, h, can in turn be estimated as:

$$h = \begin{cases} N_{Ra} > 10^9 & \dfrac{k_g}{L}\left[(0.825) + \dfrac{(0.387)N_{Ra}^{1/6}}{\left(1+\left((0.492)\frac{k_g}{\mu C_{Pg}}\right)^{9/16}\right)^{8/27}}\right]^2 \\ N_{Ra} \le 10^9 & \dfrac{k_g}{L}\left[(0.68) + \dfrac{(0.67)N_{Ra}^{1/4}}{\left(1+\left((0.492)\frac{k_g}{\mu C_{Pg}}\right)^{9/16}\right)^{4/9}}\right] \end{cases} \tag{30}$$

The material parameters here are referred to the air and the Rayleigh number being given by:

$$N_{Ra} = \frac{{\rho_g}^2 g\beta C_{Pg}\Delta T L^3}{\mu k_g} \tag{31}$$

It should be noted that Eq. (30) describes heat transfer by natural convection and does not explicitly account for the possible enhancement associated with surface condensation. The formation of liquid droplets may locally increase the effective heat-transfer coefficient; however, this effect was neglected in the present work. Simulations showed that thermal equilibration across the paperboard thickness occurs within a few minutes, whereas moisture uptake and pore saturation evolve over several hours. Therefore, the overall hydration kinetics are primarily controlled by mass-transfer processes rather than by heat-transfer limitations. Under these conditions, the effect of condensation-induced enhancement of the heat-transfer coefficient is expected to be of secondary importance and was not included in the model.

A further estimate can be made to assess the possible thermal feedback associated with latent heat release during condensation. From the experimental hydration curves, the average water uptake flux is of the order of $(10^{-6}\div10^{-5})\frac{kg}{m^2 s}$, corresponding to a latent heat flux of approximately $q_{lat} = (2\div20)\frac{W}{m^2}$. Considering the small thickness of the paperboard layer $L = 0.13\ mm$ and its dry thermal conductivity $k_s = 0.09\frac{W}{m\cdot K}$, the corresponding temperature perturbation across the wall can be estimated as $(q_{lat}L/k_s)$, giving values below approximately 0.1 K. This corresponds to a variation of local saturation vapor pressure well below 1%, which is much smaller than the experimental variability and the uncertainty associated with the fitted moisture diffusivity. This order-of-magnitude estimate supports the assumption that latent-heat feedback associated with condensation has a limited influence on the predicted hydration kinetics under the operating conditions considered in this work.

Finally, the interphase mass exchange coefficient, k_m, was obtained by the Chilton-Colburn analogy:

$$k_m = \frac{D}{k_g}\left(\frac{k_g}{\rho_g C_{Pg} D}\right)^3 h \tag{32}$$

At the interface between the paperboard wall and the inner iced water ($x=L$) the temperature is taken equal to the water temperature, and the mass flux is null (adiabatic wall for mass transfer, $\boldsymbol{n}$ being the versor orthogonal to the wall, here coincident with the $x-axis$ versor):

$$T = 0°C \tag{33}$$

$$-\boldsymbol{n}\cdot\boldsymbol{g_w} = -\boldsymbol{n}\cdot\boldsymbol{g_{lc}} = 0 \tag{34}$$

3.4. Value of parameters

Initial and boundary conditions were imposed according to the experimental setups: cups initially at ambient temperature and humidity, with their inner surface suddenly exposed to iced water (0 °C), while the outer wall exchanges heat and mass with the external atmosphere

defined by the ambient temperature and relative humidity. The external RH values used in the experiments (37% and 48%) were directly introduced as boundary conditions, and the initial sample state was assumed to correspond to equilibrium with these conditions. Temporal evolution was then simulated by integrating the governing equations across the paperboard thickness, with spatial resolution sufficient to resolve steep gradients in water content and temperature close to the surfaces.

The parameters listed in Table 3 includes structural descriptors, transport coefficients, and thermophysical constants of the dry solid. Table 4 provides complementary expressions for fluid properties, including saturation pressure as a function of temperature, gas-phase density, specific heats of dry air and water vapor, and the thermal conductivities of air, vapor, and liquid water. These temperature-dependent functions allow the simulations to capture the transient interplay between cooling, condensation, and subsequent imbibition.

3.5. Model implementation

The numerical simulations were carried out using COMSOL Multiphysics, employing the *Heat Transfer in Moist Porous Media* and *Moisture Transport in Porous Media* interfaces. The two physics were coupled using the Multiphysics node to solve the coupled heat and moisture transport equations. The domain was modeled as one-dimensional interval with a length $L = 0.13\ mm$, corresponding to the thickness of the paperboard layer (see Table 2). A physics-controlled mesh with user-defined refinement was applied, featuring a maximum element size of 0.00026 m, a maximum element growth rate of 1.05, and a narrow region resolution of 1. The coupled heat and moisture equations were solved using a fully coupled solver with a constant Newton method for the nonlinear system. The linear systems arising at each Newton iteration were solved using the direct solver PARDISO. Simulations were performed using COMSOL Multiphysics version 6.1, with each simulation lasting from 30 s to 1 min.

Table 3
Value of parameters used for simulation.

Symbol	Parameter Name	Value	UoM	Source
(a) Solid parameters and water vapor diffusivity				
ρ_{bulk}	Bulk density	991.88	$\frac{kg}{m^3}$	From experiments (section 2)
ε_p	Solid porosity	0.6	$\frac{m^3_{pores}}{m^3_{sample}}$	[18]
D	Water vapor diffusivity	2.53×10^{-5}	$\frac{m^2}{s}$	[18]
C_{Ps}	Dry solid heat capacity	1370	$\frac{J}{kg\ K}$	[19]
k_s	Dry solid thermal conductivity	0.09	$\frac{W}{m\ K}$	[19]
(b) External constraints (initial and boundary conditions) and the only fitting parameter				
T_{fixed}	Cold temperature	0	°C	Chosen parameter
$T_{external}$	External temperature	Environmental	°C	Chosen parameter
$T_{initial}$	Initial temperature	Environmental	°C	Chosen parameter
$\phi_{w,external}$	External relative humidity	Environmental		Chosen parameter
$\phi_{w,initial}$	Initial relative humidity	Environmental		Chosen parameter
D_w	Moisture diffusivity	1.11×10^{-12}	$\frac{m^2}{s}$	Fitting parameter

Table 4
Parameters used to describe water and moist air behavior.

Symbol	Parameter Name, [Units of Measurements] / Value or expression
M_{water}	Molar mass of water, [kg /mol] (0.018)
M_{air}	Molar mass of dry air, [kg /mol] (0.02897)
X_v	Molar fraction of water vapor, [dimensionless] $X_v = \frac{\omega_v/M_{water}}{\omega_v/M_{water} + \omega_{air}/M_{air}}$
$P_{sat}(T)$	Saturation Pressure, [Pa] $(610.7)\cdot 10^{7.5\frac{T-273.15\ [K]}{T-35.85\ [K]}}$
ρ_{water}	Density of pure liquid water, $[kg/m^3]$ (1000)
ρ_g	Density of the gas phase, $[kg/m^3]$ $\frac{p_A(M_{air} - X_v(M_{air} - M_{water}))}{RT}$
C_{Pl}	Specific heat capacity of liquid water, [J /(kg ·K)] [20] $C_{Pl}(T)$ = interpolation from tabulated data
C_{Pg}	Moist air heat capacity at constant pressure, [J /(kg ·K)] $(1 - X_v)C_{Pa} + X_vC_{Pv}$
C_{Pa}	Heat capacity at constant pressure of dry air, [J /(kg ·K)] $(1047.64) - (0.37)T + (9.45\cdot10^{-4})T^2 - (6.024\cdot10^{-7})T^3 + (1.28\cdot10^{-10})T^4$
C_{Pv}	Heat capacity at constant pressure of water vapor, [J /(kg ·K)] $(4653.75) - (31.45)T + (0.14)T^2 - (3.31\cdot10^{-4})T^3 + (4.27\cdot10^{-7})T^4 - (2.88\cdot10^{-10})T^5 + (7.94\cdot10^{-14})T^6$
k_l	Thermal conductivity of liquid water, [W /(mg ·K)] [20] $k_l(T)$ = interpolation from tabulated data
k_g	Moist air thermal conductivity, [W /(mg ·K)] $(1 - X_v)k_a + X_vk_v$
k_a	Thermal conductivity of dry air, [W /(mg ·K)] $(-0.0023) + (1.15\cdot10^{-4})T - (7.90\cdot10^{-8})T^2 + (4.12\cdot10^{-11})T^3 - (7.44\cdot10^{-15})T^4$
k_v	Thermal conductivity of water vapor, [W /(mg ·K)] $(0.0019) + (3.57\cdot10^{-5})T + (6.43\cdot10^{-8})T^2 + (5.36\cdot10^{-12})T^3 - (9.97\cdot10^{-15})T^4$

4. Results and discussion

4.1. Water on paper adsorption isotherm and its extension

Fig. 1 shows the moisture adsorption isotherm for paperboard materials, obtained from data available in the literature. For values of water mass fraction at $\phi_w < 0.9$, the data represent the average of three independent isotherms taken from the work of [18,21,22]. Although specific isotherm at 0 °C, closer to the actual operating conditions of the material, were sought, the differences between the isotherms at 0 °C and 22 °C were found to be negligible. Therefore, the isotherms at 22 °C were considered adequate for the purpose of this study.

The literature isotherms typically reported up to high relative humidity values, but below the saturation point of water vapor. As well documented in the field of sorption science, paper and fibrous cellulosic substrates exhibit the typical sigmoidal curve, with three distinct regions: the initial low-relative humidity range where adsorption is mainly monomolecular, the intermediate range characterized by multilayer adsorption and capillary condensation in mesopores, and the high-relative humidity range where water uptake rises sharply due to the progressive filling of larger pores and capillaries. In most literature studies, however, the isotherm is truncated before reaching relative humidities close to or beyond saturation, thereby limiting the description to the hygroscopic domain.

By contrast, our experimental campaign extended the investigation beyond this classical range, exploring conditions of supersaturation ($\phi_w > 1.0$), which are practically relevant whenever materials are exposed to condensation environments. The additional data point in Fig. 1, derived from our own measurements, clearly shows a discontinuity with respect to the literature isotherm: once the system is brought

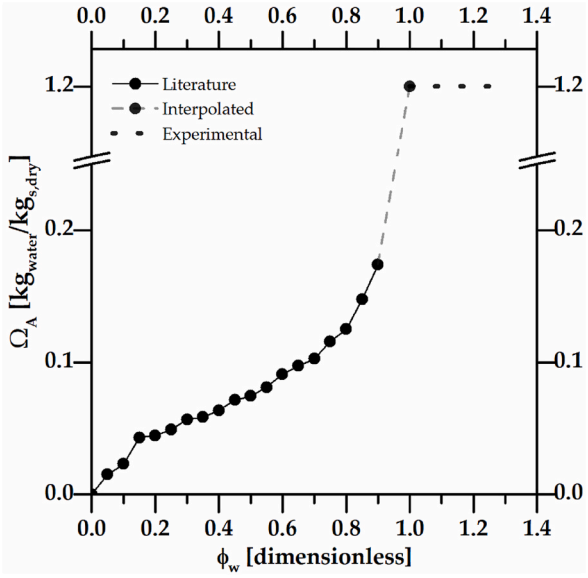

Fig. 1. Adsorption isotherm (25 °C) for humidity on paperboard. The data for $\phi_w < 0.9$ were taken from literature (see text for references), the value $\Omega_A = 1.2\ \frac{kg_{water}}{kg_{s,dry}}$ is for $\phi_w > 1.0$ (supersaturation) and has been determined in the present work, the dashed gray line between the values $\phi_w = 0.9$ and $\phi_w = 1.0$ is a linear interpolation.

into a supersaturated atmosphere, the equilibrium water content on a dry basis increases dramatically, reaching values as high as $\Omega_A \approx 1.2\ kg_{water}/kg_{s,dry}$. This level of hydration is far above what is predicted by conventional sorption models and indicates that condensation processes dominate over purely adsorptive mechanisms. In other words, while the literature data describe the hygroscopic uptake governed by fiber–water interactions and pore filling, our measurements could be interpreted in the sense that, under supersaturated conditions, surface condensation and liquid imbibition become the prevailing mechanisms, thereby altering the moisture balance of the material.

This phenomenon is further confirmed by the photos shown in Fig. 2, which documents the hydration experiments conducted under exposure to external humid air, while the cups are filled with iced water. The time-lapse images (and corresponding thermo-gravimetric data) provide direct evidence of progressive surface condensation on the paperboard wall, followed by liquid penetration into the porous fiber network. The dynamics observed experimentally show that once the ambient air approaches dew point conditions, the material is rapidly wetted not only by adsorption but also by the accumulation of liquid water films on the surface, which are most probably also drawn into the bulk through capillary forces. The combination of adsorption, capillary condensation, and macroscopic liquid imbibition explains the sudden rise in the measured water fraction, which can be described with the sharp departure lower relative humidity data point from the literature isotherm in Fig. 1.

From a physical standpoint, the comparison between the two figures emphasizes the critical role of relative humidity in the vicinity of saturation. While in the hygroscopic regime water uptake scales gradually with RH, in the supersaturated regime even a small excess beyond $\phi_w = 1.0$ triggers a qualitatively different mechanism, leading to orders-of-magnitude higher hydration levels. For paper-based packaging materials, this has important implications: the mechanical strength, dimensional stability, and barrier properties are all strongly dependent on moisture content, and the transition from adsorption-controlled to condensation-controlled hydration may mark the threshold between acceptable and unacceptable performance in service conditions.

In summary, the juxtaposition of Figs. 1 and 2 highlights that literature sorption data, though accurate in describing equilibrium in subsaturated atmospheres, are insufficient to predict the material's behavior under practical exposure to condensation environments. Our experiments extend the understanding by quantifying the extent of water uptake under supersaturation and by directly visualizing the hydration process. The findings underscore the necessity of considering not only hygroscopic sorption but also condensation and imbibition phenomena when assessing the durability and functional performance of paper-based laminates and containers in high-humidity or condensation-prone applications.

4.2. Hydration experiments

Fig. 3 shows the time evolution of the average water fraction on a dry basis, $\langle \Omega_A \rangle$, measured in two experimental campaigns carried out with "small" (A) and "large" (B) cups. To ensure reliability, each test was performed in triplicate: symbols indicate the mean values and the error bars correspond to the standard deviation. Each point therefore represents the integrated measurement after a defined exposure interval, with environmental conditions kept constant throughout each series (22.4 °C, RH 37% and 24.0 °C, RH 48%). Accordingly, the figure captures the temporal dynamics of hydration under fixed boundary conditions rather than variations with ambient relative humidity.

The data exhibit a clearly monotonic trend that can be described in two regimes. In the initial stage (within the first tens of minutes to about 1 h), $\langle \Omega_A \rangle$ increases rapidly, reflecting fast uptake processes such as surface adsorption and the filling of the most accessible capillaries. This is followed by a slower growth regime: between one and 6 h the slope decreases, suggesting that diffusion and capillary transport in less accessible pores control the kinetics. For large times, the measurements approach a plateau, meaning that a fully stabilized equilibrium value is reached within the experimental time window. The reproducibility among replicates confirms the systematic nature of this two-stage hydration behavior.

The two experimental series also reveal quantitative differences in both the initial uptake rate and the absolute hydration level achieved after several hours. These differences are consistent across replicates,

Fig. 2. The evolution of water uptake with time. From the left, photo taken after 30 min, 1 h, 2 h, and 6 h of the pouring of iced water. The surface condensation is clearly visible.

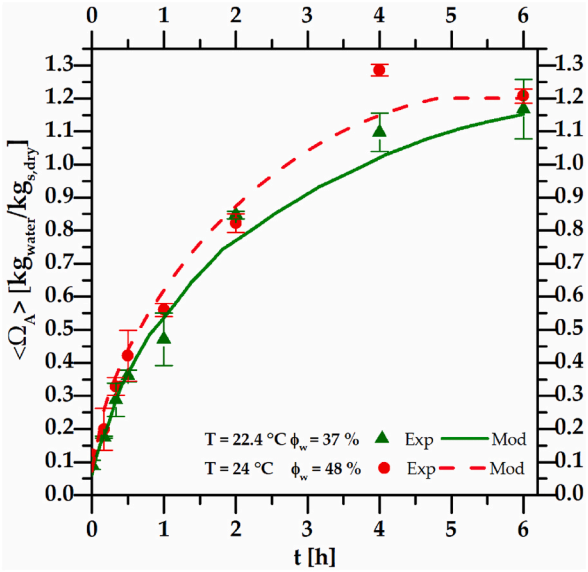

Fig. 3. The two absorption experiments performed in this work, working with A "small" and B "large" cups, in slightly different environment conditions (A: RH = 37% at 22.4 °C; B: RH = 48% at 24.0 °C). Symbols are experimental data (carried out in triplicate, average values are reported, error bars are standard deviations) and lines are modeling results. Values are expressed as average mass fraction (on dry basis) $\langle \Omega_A \rangle$ evolution with time.

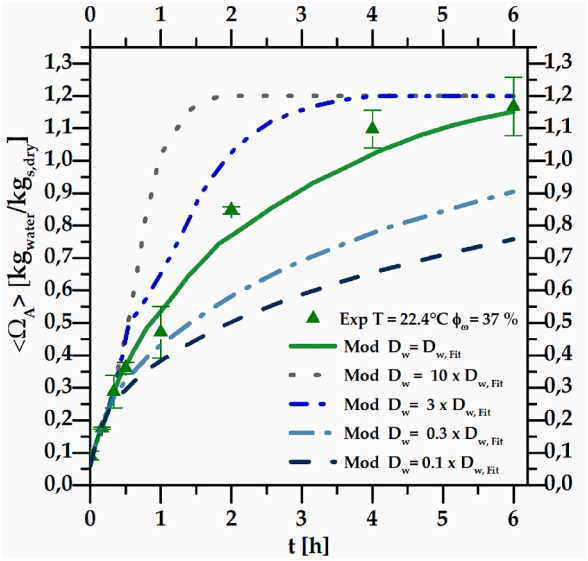

Fig. 4. Sensitivity analysis of the model predictions to the moisture capillary diffusivity D_w. Experimental data are compared with simulations obtained using different values of the fitted parameter D_w.

appearing as vertical shifts and slight changes in slope. Error bars remain relatively small overall, but they tend to enlarge during the periods of rapid water accumulation, which can be attributed to the stochastic nature of local condensation or imbibition events at the fiber network scale.

In summary, the data points in Fig. 3 clearly and reproducibly document that, under constant external conditions, laminated paperboard undergoes a time-dependent hydration process characterized by an initial rapid uptake followed by a slower, diffusion-controlled regime. These experimental findings provide the empirical foundation against which model predictions can be compared.

4.3. Model simulations of experimental conditions

4.3.1. Model implementation and parameters

The simulations of the model proposed in this work were carried out by numerically solving the coupled heat and mass transfer equations formulated in Section 3, using as input the structural, thermophysical, and environmental parameters summarized in Tables 3 and in Table 4. The model builds on a continuum description of the paperboard substrate, treated as a porous fibrous solid characterized by bulk density, porosity, and pore geometry. Water transport is represented by a dual mechanism: vapor diffusion through the interconnected pore network and capillary liquid flow. Vapor transport is described by an effective diffusivity, defined as the product of the free-air diffusivity and a correction factor accounting for porosity and tortuosity, while liquid water transport is described by a capillary diffusivity term. This latter parameter, D_w, was treated as the only adjustable quantity, calibrated against experimental hydration kinetics, whereas all other physical constants were either measured experimentally (bulk density, paperboard thickness) or retrieved from the literature.

The moisture capillary diffusivity, $D_w = 1.11 \cdot 10^{-12} m^2/s$, was indeed the only adjustable parameter of the model. To assess the influence of this parameter on model predictions, a sensitivity analysis was performed by varying D_w around its calibrated value. The results, reported in Fig. 4, show that D_w primarily affects the rate of water uptake, with larger values leading to faster hydration kinetics and smaller values resulting in slower uptake. However, the characteristic two-stage behavior of the process is preserved over the entire range investigated, indicating that the qualitative predictions of the model are robust with respect to moderate variations of D_w.

Although the calibrated value of D_w provides good agreement with the experimental data, some uncertainty remains associated with its estimation. The sensitivity analysis presented in Fig. 4 illustrates the influence of this parameter on the predicted hydration kinetics and provides an indication of the robustness of the model predictions with respect to variations of the fitted diffusivity.

The governing mass balance equation (10) accounts for the time derivative of the local water concentration, expressed through the sorption equation linking pore saturation and external relative humidity. Fluxes of both vapor and liquid water are then computed through pseudo-Fickian expressions (equations (11) and (12)), allowing the simultaneous representation of hygroscopic uptake and capillary imbibition. The heat balance equation (15) is solved concurrently, with an effective volumetric heat capacity incorporating solid, vapor, and liquid fractions. Thermal conductivity is likewise expressed as a weighted average of the three phases, modulated by porosity and saturation equation (18). Latent heat effects are explicitly included through the evaporation term, ensuring that condensation and evaporation phenomena are correctly coupled to the local thermal field.

It should be emphasized that condensation is not represented through an explicit source term in the governing equations. Instead, it emerges naturally from the coupling between heat transfer, vapor transport, and the sorption relationship adopted for the porous medium. As the paperboard wall is cooled by the cold beverage, the local vapor concentration may exceed the saturation value, leading to supersaturated conditions ($\varphi > 1$). Under these conditions, the model predicts a progressive increase in liquid saturation within the pore network, which is interpreted as condensation followed by capillary-driven imbibition. Consequently, the vapor boundary condition imposed at the external surface acts as the driving force for moisture ingress, while the transition from vapor-dominated transport to liquid accumulation is captured through the supersaturation-dependent evolution of liquid saturation.

Overall, the simulations represent a mechanistic reconstruction of the hydration dynamics observed experimentally: they start from well-characterized material and environmental parameters, introduce only a single fitting coefficient for liquid transport, and solve the coupled energy and mass balances consistently across the multilayer wall. This framework makes it possible not only to reproduce the time evolution of

water uptake under the conditions tested but also to extend predictions to alternative climates or cup geometries, as later sections demonstrate.

Although the model is formulated as a fully coupled heat- and mass-transfer problem, the relative importance of the two transport mechanisms is not known a priori and must be assessed through simulation. For this reason, the following section first examines the characteristic evolution of the thermal and moisture fields before discussing the hydration kinetics of the paperboard.

4.3.2. Hydration evolution simulations

The curves shown in Fig. 3 represent the outcome of the numerical simulations carried out with the coupled heat and mass transfer model introduced in Section 3, using the parameter sets listed in Tables 3 and 4. In both panels (A: small cup, B: large cup), the continuous lines correspond to the predicted temporal evolution of the mean water content, $\langle \Omega_A \rangle$, across the paperboard wall thickness, under the same external boundary conditions as in the experiments. The general trend of the curves is consistent: an initial steep rise in hydration, followed by a gradual deceleration towards a quasi-asymptotic regime. This two-stage behavior arises naturally from the model formulation. In the first few minutes after exposure, the imposed temperature difference between the cold inner surface (in contact with iced water) and the warmer ambient air drives a rapid condensation of vapor at the inner boundary. The model captures this by means of the sorption isotherm extended to supersaturated conditions, which results in a strong gradient in pore saturation near the inner surface. As a consequence, the effective diffusivity for water transport is large, leading to the fast increase in mean water content that is visible in the early portion of the simulated curves.

As time proceeds, the steepest gradients in both temperature and vapor pressure progressively relax. Heat transfer through the wall reduces the driving force for condensation, while the porous network becomes increasingly saturated, lowering the effective diffusivity for both vapor and liquid transport. The model curves thus show a clear transition towards a slower growth regime, where $\langle \Omega_A \rangle$ increases only marginally with time.

Another relevant aspect captured by the simulations is the dependence on ambient relative humidity. The curves corresponding to the two boundary conditions (RH = 37% at 22.4 °C and RH = 48% at 24.0 °C) are clearly separated: higher external humidity translates into greater driving force for vapor diffusion and, consequently, higher equilibrium hydration levels. The difference between the two sets of curves grows with time, as the contribution of imbibed liquid water accumulates in the porous matrix. This sensitivity demonstrates that the model, while relying on a single fitting parameter for liquid diffusivity, is able to reproduce the systematic dependence of hydration dynamics on external humidity.

Particularly noteworthy is the ability of the model to reproduce the experimentally observed transition from an initial rapid hydration stage to a subsequent slower transport-controlled regime, despite the use of a single adjustable parameter.

Overall, the simulated curves of Fig. 3 provide a mechanistic explanation for the experimental observations. The initial steep slopes correspond to rapid condensation at the cold surface, followed by transport-driven imbibition into the wall; the subsequent flattening reflects the progressive reduction of driving forces and the approach to local equilibrium. Differences between ambient humidity levels are quantitatively reproduced, highlighting the robustness of the model implementation and its ability to capture both the kinetics and the asymptotic states of hydration under fixed boundary conditions.

4.3.3. Gain insight into the heat and mass transport

Fig. 5 compares the simulated temporal evolution of the temperature distribution across the paperboard wall with that of the corresponding water concentration. A striking feature of the results is the difference in characteristic time scales: while the temperature profile becomes nearly flat within a very short period after exposure to iced water, the evolution of water concentration extends over much longer times. Immediately after contact, the steep thermal gradient between the cold inner surface and the ambient air drives rapid heat conduction across the porous structure. Due to the relatively small thickness of the wall and the low thermal mass of the fibrous matrix, thermal equilibration occurs quickly: within a matter of minutes, the calculated profiles indicate that the temperature throughout the wall is nearly uniform. This flattening suggests that the thermal field can be treated as quasi-steady for most of the hydration process.

By contrast, the redistribution of water within the porous medium is much slower. The concentration profiles evolve over several hours, displaying a progressive penetration of moisture from the inner surface towards the bulk. This delayed response reflects the fundamentally different transport mechanisms controlling water movement. Unlike heat, which diffuses rapidly through both solid and fluid phases, water uptake is limited by sorption kinetics, capillary condensation, and liquid imbibition into a complex pore network. These processes involve higher resistance and stronger dependence on local saturation, resulting in characteristic times that are one to two orders of magnitude longer than thermal equilibration.

The juxtaposition of the two fields in Fig. 5 has an important

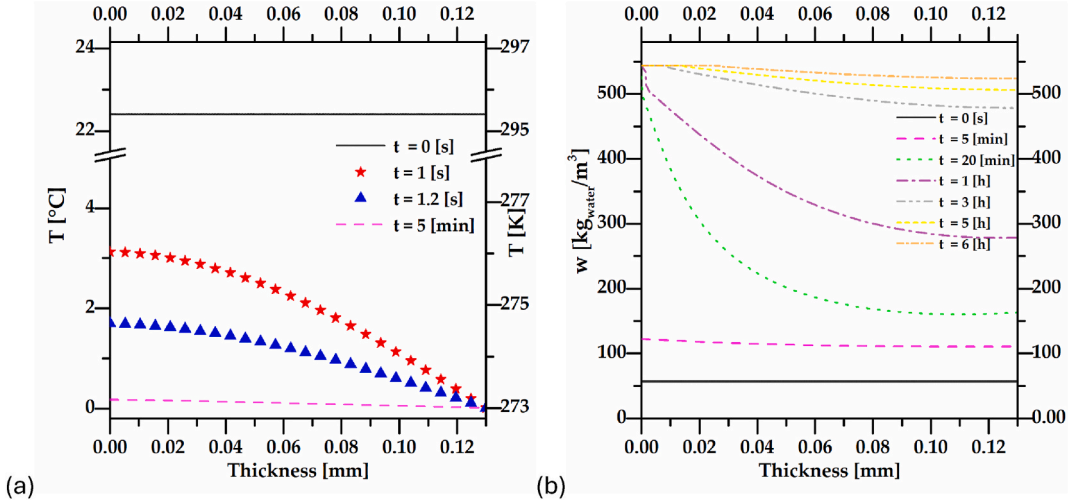

Fig. 5. On the left (a): temperature profiles along the paperboard thickness with time; on the right (b): water concentration profiles along the paperboard thickness with time.

implication for modeling: once the initial temperature drop has been accounted for, further changes in hydration occur under nearly isothermal conditions. In practice, this means that the coupled heat transfer can be neglected without significant loss of accuracy, allowing the model to be simplified to a mass-transport-driven formulation. Such an assumption is supported by the simulations, which clearly demonstrate that the dominant dynamics of interest—namely the increase in average water fraction—are not constrained by thermal limitations but by the kinetics of vapor condensation and subsequent imbibition.

In summary, Fig. 5 highlights a fundamental separation of time scales: thermal equilibration in the paperboard wall is extremely fast and essentially complete within minutes, whereas the build-up of water concentration is much slower and continues for several hours. Recognizing this difference is crucial for simplifying the model and focusing on the processes that truly govern the material's hydration behavior.

Fig. 6 presents the simulated profiles of relative humidity, ϕ_w, and liquid saturation, s_L, across the paperboard wall, using the same temporal scale adopted in Fig. 5b for water concentration. This direct comparison highlights the different roles of vapor-phase humidity and liquid water accumulation in controlling the overall hydration dynamics. Immediately after the inner wall is exposed to iced water, the model predicts a sharp increase of local relative humidity in the pores adjacent to the cold surface. Roughly after 20 min, ϕ_w exceeds unity, marking the onset of supersaturation. This condition triggers condensation, which in turn initiates the build-up of liquid saturation within the pore space. The temporal correspondence between ϕ_w rising above 1 and the subsequent increase in s_L both confirm that condensation is the mechanism driving the transition from vapor-dominated to liquid-dominated water uptake.

The evolution of s_L is particularly instructive. Starting from an initially dry state, saturation rises progressively as liquid water nucleates and invades the pore network. Over the timescale of several hours, s_L approaches an asymptotic value close to 0.95, meaning that approximately 95% of the available pore volume becomes filled with liquid water. This nearly complete pore filling is consistent with the high hydration levels measured experimentally under supersaturated conditions and correlate with the sudden increase in average water fraction noted in Fig. 3. The persistence of such high saturation confirms that, once condensation begins, the paperboard does not simply adsorb additional molecular layers but undergoes capillary imbibition, leading to a structural state where the paperboard becomes almost completely filled with liquid water.

It is also important to note that the timescale for these processes is long compared with thermal equilibration, as already shown in Fig. 4a. While temperature profiles flatten within minutes, the profiles of ϕ_w and s_L continue evolving over hours, indicating that mass transfer processes dominate the kinetics of hydration. The use of the same temporal axis for Fig. 5b and 6 makes this contrast evident: heat transfer can be neglected after the initial transient, while vapor condensation and liquid imbibition remain active for the entire duration of the simulation.

In summary, Fig. 6 demonstrates how local supersaturation ($\phi_w > 1$) suggesting that a large fraction of the available pore volume may become occupied by liquid water, with liquid saturation rising to nearly 95%. This coupling between vapor humidity and liquid occupancy provides a mechanistic explanation for the dramatic water uptake observed experimentally and confirms that under condensation-prone conditions the porous structure of the paperboard is almost completely filled with liquid water.

4.4. Model simulations of different environmental conditions

Fig. 7 illustrates the results of the numerical simulations performed

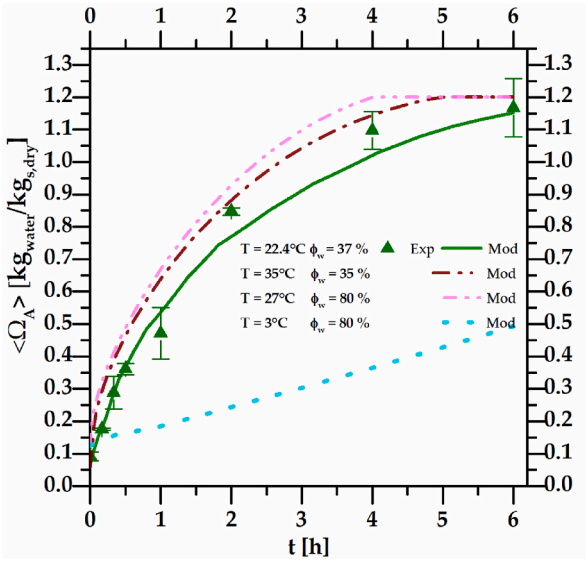

Fig. 7. Water up-take in a paper cup filled with cold soda in different environmental conditions (dry winter: 22.4 °C, RH 37%; humid winter: 3 °C, RH 80%; dry summer: 35 °C, RH 35%; humid summer: 27 °C, RH 80%).

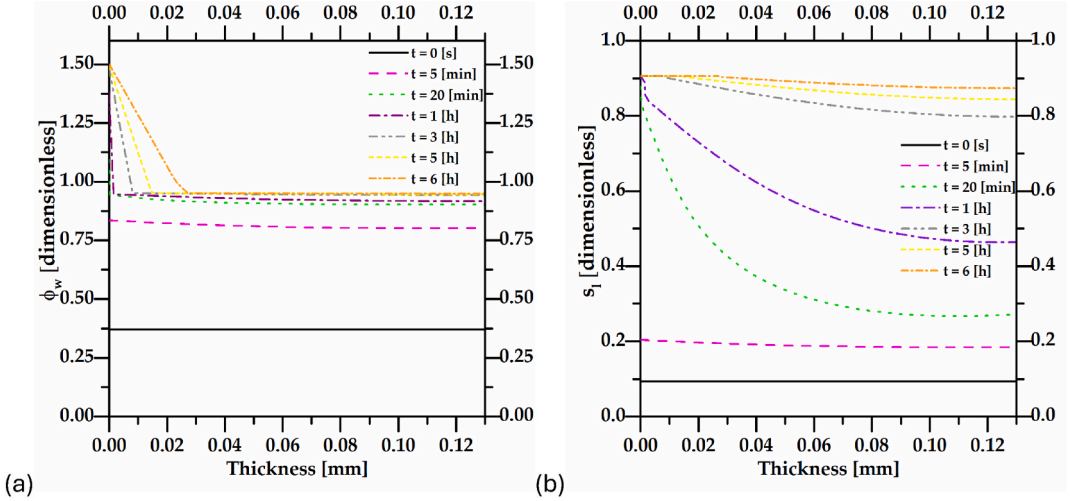

Fig. 6. On the left (a): relative humidity profiles along the paperboard thickness with time; on the right (b): liquid saturation profiles along the paperboard thickness with time.

under a range of ambient conditions, chosen to represent typical seasonal and climatic scenarios. Unlike the previous figures, where the focus was on reproducing the specific laboratory experiments, here the intent is to explore the model's predictive capability by subjecting the cup walls to combinations of temperature and relative humidity that mimic realistic environmental situations. Four representative cases are displayed: a dry winter climate, a humid winter climate, a dry summer climate, and a humid summer climate. Together, they provide a synthetic picture of how the same paperboard structure would respond when used in very different geographical locations and times of the year.

The simulations show that in dry winter conditions (low temperature and low relative humidity), the paperboard wall accumulates only a modest amount of water over time. The low vapor content of the surrounding air limits the driving force for condensation, and the cold external atmosphere enhances heat losses, thereby reducing the temperature gradient across the wall. Under such conditions, the model predicts hydration levels that remain relatively low and stable, suggesting that cups used in dry continental winters would maintain their mechanical integrity for extended periods.

By contrast, in humid winter conditions (low temperature but high relative humidity), water uptake is significantly enhanced. The cold air holds less vapor in absolute terms, but its high relative humidity ensures that the external surface of the wall remains close to saturation. The model reproduces this by predicting a faster initial uptake and higher equilibrium water content than in the dry winter scenario. This corresponds to climates such as coastal or maritime winters, where fog or mist is common, and where paper-based cups may become more vulnerable to moisture-related weakening.

Moving to summer conditions, the simulations reveal a different interplay between temperature and humidity. In a dry summer climate (high temperature, low relative humidity), the high ambient temperature tends to reduce the relative difference between the cold inner surface and the external environment, leading to moderate condensation at the iced-water interface. The low external humidity limits additional water up-take, so the predicted hydration levels remain intermediate: higher than in the dry winter case but still bounded. This scenario is reminiscent of hot, arid environments, such as desert or continental interiors, where cups are exposed to elevated air temperatures but relatively dry atmospheres.

Finally, in humid summer conditions (high temperature and high relative humidity), the model predicts the most critical behavior. Here, the external air is both warm and moisture-laden, maximizing the driving force for condensation and diffusion. The simulated hydration curves rise rapidly and reach the highest values among all cases, indicating that paper cups used in tropical or subtropical climates would be especially prone to water uptake and loss of structural performance. This prediction aligns with common experience: in humid summers, condensation tends to bead heavily on cold surfaces, and porous materials readily absorb liquid water.

Altogether, the simulations in Fig. 7 provide a compelling demonstration of how the same material, with identical structure and properties, may perform very differently depending on the climatic context. The model allows us to imagine the behavior of paper cups around the world: from the relative safety of a dry alpine winter to the challenges posed by a muggy tropical summer. This exercise highlights the broader applicability of the modeling framework and underlines the importance of considering environmental variability when assessing the durability and functionality of paper-based laminates for food and beverage applications.

5. Conclusions

The present work addressed the complex problem of heat and mass transfer in paper cups filled with cold beverages (still limiting the attention to the two-layers design, which is primarily intended for use with hot beverages), with a particular focus on the hydration dynamics of the paperboard layer under condensation-prone conditions. The research effort followed a structured path comprising five major steps: (i) extension of the water–paper adsorption isotherm to supersaturated conditions by experimental measurement; (ii) execution of dynamic absorption experiments on cups filled with iced water; (iii) development of a coupled heat-and-mass transport model; (iv) calibration of the model against the experimental data; and (v) application of the validated model as a predictive tool to simulate hydration under diverse environmental conditions.

The first key achievement of this study was the extension of the adsorption isotherm beyond the classical hygroscopic domain. Literature data typically describe equilibrium uptake of moisture by paper only up to relative humidities below 100%. Our experiments, by contrast, explicitly investigated the supersaturated regime ($\phi_w > 1$), which is practically relevant whenever condensation occurs. The additional experimental points collected in this regime revealed a sharp discontinuity from the literature isotherm: once condensation takes place, the equilibrium water content on a dry-basis increases dramatically, reaching values of $\Omega_A \approx 1.2\ \mathrm{kg_{water}/kg_{s,dry}}$. This observation supports the interpretation that adsorption alone is insufficient to explain moisture uptake near saturation and that condensation and liquid imbibition into the fiber network should be considered.

The second important contribution came from the dynamic hydration experiments. By exposing both small and large cups to iced-water filling, and by monitoring water content over time, it was possible to capture the temporal evolution of hydration under fixed ambient conditions. The results consistently showed a two-stage process: an initial rapid uptake within the first hour, associated with surface condensation and pore filling in easily accessible regions, followed by a slower diffusion- and capillarity-controlled regime lasting several hours. The reproducibility of the experiments, with relatively small error bars across replicates, confirmed the robustness of this experimental design and provided a reliable benchmark for model validation.

Building on this experimental basis, the third step was the formulation of a mechanistic model. The model describes the paperboard as a porous medium where water transport occurs via two concurrent pathways: vapor diffusion through the pore network, and capillary imbibition of liquid water. Vapor diffusion is quantified using an effective diffusivity corrected for porosity and tortuosity, while liquid transport is represented by a capillary diffusivity term. The sorption equation linking local relative humidity to water concentration ensures consistency with adsorption–condensation physics, while the heat balance equation accounts for conduction, effective heat capacity, and latent heat of evaporation. Importantly, simulations demonstrated that thermal equilibration occurs much faster than moisture uptake, allowing heat transfer to be neglected beyond the first minutes and simplifying the problem to a mass-transport-driven one.

The model was then fitted against the experimental hydration curves using a single adjustable parameter, the liquid diffusivity D_w. All other quantities—structural properties, diffusivities, and thermophysical constants—were either measured directly or taken from literature. Despite this minimal fitting, the agreement between simulations and experiments was very good. The model successfully captured both the initial steep rise and the subsequent slower evolution of average water fraction, as well as the dependence of equilibrium hydration levels on ambient humidity. This confirmed the reliability of the theoretical framework and validated the underlying assumptions on coupled vapor and liquid transport. Since moisture uptake is known to reduce the stiffness and structural integrity of paperboard materials, the predicted hydration levels may also be interpreted as an indicator of potential mechanical performance degradation during service. One of the most interesting outcomes of the simulation is that the timescale of heat transfer is very fast with comparison to the mass transfer, therefore the process can be seen as a quasi-isothermal process, and the heat transfer phenomena can be neglected. A limitation of the present study is that the

predicted liquid saturation profiles within the paperboard were inferred from the model and were not directly validated through imaging or other spatially resolved experimental techniques; therefore, the internal distribution of liquid water should be regarded as a model-based prediction consistent with the observed hydration kinetics.

Finally, the model was employed as a predictive tool to explore hydration dynamics under environmental conditions not directly tested in the laboratory. Simulations covering representative "climatic" cases—dry winter, humid winter, dry summer, and humid summer—demonstrated how the same paper cup may exhibit dramatically different behaviors depending on the ambient temperature and relative humidity. In dry winter conditions, hydration remained low and stable; in humid winters, uptake increased significantly due to external air near saturation; in dry summers, the effect was intermediate, with moderate water ingress; and in humid summers, the model predicted the highest uptake, with saturation levels approaching complete pore filling. These predictions aligned with practical experience and illustrated the broader utility of the model in anticipating cup performance in different geographic and seasonal scenarios. While the predicted evolution of liquid saturation is consistent with the measured hydration kinetics, direct experimental validation of the internal saturation profiles was beyond the scope of the present study.

In summary, the work has produced three main outcomes. First, the experimental campaign generated new data extending the adsorption isotherm into the supersaturation regime and documenting dynamic hydration under controlled conditions. Second, a robust and physically grounded model was developed, calibrated, and validated, requiring only one fitting parameter to reproduce the observed kinetics. Third, the predictive capability of the model was demonstrated by applying it to realistic environmental conditions, showing its ability to anticipate condensation and water uptake in diverse climates worldwide.

These contributions not only advance the scientific understanding of moisture transport in paper-based laminates but also have direct industrial implications, even if limited to 2-layers paper cups, which are of limited use for cold beverages, being the 3-layers preferred. By capturing the transition from hygroscopic adsorption to condensation-driven flooding of pores, the model provides a rational tool for predicting cup durability and barrier performance under realistic service conditions. This predictive capacity is essential as a tool for designing improved materials, optimizing coatings, even to evaluate the performance of biodegradable alternatives to polyethylene, and more sophisticated design (thinking of 3-layers paper cups). More broadly, the integrated experimental–modeling approach presented here establishes a framework that can guide the engineering of sustainable, reliable paper-based packaging systems for global markets.

CRediT authorship contribution statement

Raffaella De Piano: Data curation, Investigation, Methodology, Writing – review & editing. **Diego Caccavo:** Investigation, Methodology, Writing – review & editing. **Antonia Calabrese:** Investigation, Methodology, Writing – review & editing. **Anna Angela Barba:** Conceptualization, Methodology, Supervision, Writing – review & editing. **Anette Larsson:** Conceptualization, Formal analysis, Writing – review & editing. **Gaetano Lamberti:** Conceptualization, Supervision, Writing – original draft, Writing – review & editing.

Declaration of competing interest

The authors declare that they have no known competing financial interests or personal relationships that could have appeared to influence the work reported in this paper.

Nomenclature

Variable	Name	Units of measurement
Ω_A	water mass fraction (on dry basis)	$\frac{kg_{water}}{kg_{s,dry}}$
ε_p	solid porosity	$\frac{m^3_{pores}}{m^3_{sample}}$
$(\rho C_P)_{eff}$	'effective' heat capacity	$\frac{J}{m^3 K}$
ρ_{bulk}	bulk density of the sample	$\frac{kg_{s,dry}}{m^3}$
ρ_g	density of gas phase	$\frac{kg_{g,tot}}{m^3}$
ρ_{water}, ρ_l	density of pure liquid water	$\frac{kg_{water}}{m^3}$
ρ_{wet}	wet density of the sample	$\frac{kg_{s,wet}}{m^3}$
τ	pore tortuosity	dimensionless
ω_A	water mass fraction (on wet basis)	$\frac{kg_{water}}{kg_{s,wet}}$
ω_v	mass fraction of water in gas phase	$\frac{kg_{water}}{kg_{g,tot}}$
ϕ_w	relative humidity (of the gas phase)	dimensionless
D	diffusivity of water vapor in air	$\frac{m^2}{s}$
D_{eff}	effective diffusivity of vapor	$\frac{m^2}{s}$
D_w	moisture capillary diffusivity	$\frac{m^2}{s}$
M_w	water molar mass	$\frac{kg_{water}}{mol_{water}}$
$P_{sat}(T)$	saturation pressure of water in air	Pascal
P_v	partial pressure of water vapor in gas phase	Pascal
$c_{sat}(T)$	saturation concentration of water vapor in gas phase	$\frac{mol_{water}}{m^3}$

(*continued on next page*)

(*continued*)

c_v	(molar) concentration of water vapor in gas phase	$\frac{\text{mol}_{\text{water}}}{\text{m}^3}$
$\boldsymbol{q}$	conductive heat flux	$\frac{\text{W}}{\text{m}^2}$
Q_{parz}	heat flow rate due to partial enthalpy transfer	$\frac{\text{W}}{\text{m}^3}$
Q_{evap}	heat flow rate due to evaporation	$\frac{\text{W}}{\text{m}^3}$
s_l	liquid saturation	$\frac{\text{m}^3_{\text{liquid}}}{\text{m}^3_{\text{pores}}}$
$\boldsymbol{g_w}$	water vapor flux in the gas phase	$\frac{\text{kg}_{\text{water}}}{\text{m}^2\text{s}}$
$\boldsymbol{g_{lc}}$	water capillary flux in the liquid phase	$\frac{\text{kg}_{\text{water}}}{\text{m}^2\text{s}}$
w	water concentration	$\frac{\text{kg}_{\text{water}}}{\text{m}^3}$

Data availability

No data was used for the research described in the article.

References

[1] P.K. Kunam, D. Ramakanth, K. Akhila, K.K. Gaikwad, Bio-based materials for barrier coatings on paper packaging, Biomass Convers. Biorefinery 14 (2024) 12637–12652.

[2] F. Jahangiri, A.K. Mohanty, M. Misra, Sustainable biodegradable coatings for food packaging: challenges and opportunities, Green Chem. 26 (2024) 4934–4974.

[3] A.J. Lindstad, A.Å. Hansen, K.D. Li, M.K. Pettersen, Material properties of paperboard with biodegradable and nonbiodegradable coatings affected by storage conditions and contact with selected food products, Packag. Technol. Sci. 38 (2025) 379–392.

[4] H. Derluyn, H. Janssen, J. Diepens, D. Derome, J. Carmeliet, Hygroscopic behavior of paper and books, J. Build. Phys. 31 (2007) 9–34.

[5] FORTUNE BUSINESS INSIGHTS, *Paper Cups Market Size, Share & Industry Analysis, by Type (Hot Paper Cups and Cold Paper Cups), by Wall Type (Single Wall Paper Cups and Multiple Wall Paper Cups), by End-User (Household, Quick Service Restaurants (QSR), and Others), and Regional Forecast, 2025-2032* [Online]. Fortune Business Insights, 2025. Available: https://www.fortunebusinessinsights.com/paper-cups-market-105010. (Accessed 29 August 2025).

[6] STRAITS RESEARCH, Paper cups market size, share & trends analysis report by cup type, by end-user industry, by wall type, by cup capacity, by sales channel and by region, Forecasts, 2025-2033 [Online]. Straits Research. Available: https://straitsresearch.com/report/paper-cups-market, 2025. (Accessed 29 August 2025).

[7] PRECEDENCE RESEARCH, Paper cups market size and forecast 2025 to 2034 [Online]. Available: https://www.precedenceresearch.com/paper-cups-market, 2025. (Accessed 29 August 2025).

[8] GRAND VIEW RESEARCH, Disposable cups market size, share & trends analysis report by product, by end-use, by region, and segment forecasts, 2025 - 2030 [Online]. Grand View Research. Available: https://www.grandviewresearch.com/industry-analysis/disposable-cups-market, 2025. (Accessed 29 August 2025).

[9] L. Carlsson, Out-of-plane hygroinstability of multi-ply paperboard, Fibre Sci. Technol. 14 (1981) 201–212.

[10] G. Marin, Impact of Paperboard Deformation and Damage Mechanisms on Packaging Performance, KTH Royal Institute of Technology, 2023. PhD Thesis.

[11] A. Cornaggia, T. Gajewski, A. Knitter-Piątkowska, T. Garbowski, Influence of humidity and temperature on mechanical properties of corrugated board - numerical investigation, Bioresources 18 (2023) 7490–7509.

[12] R.R. Samal, H.S. Navani, S. Saha, B. Kisan, U. Subudhi, Evidence of microplastics release from polythene and paper cups exposed to hot and cold: a case study on the compromised kinetics of catalase, J. Hazard Mater. 454 (2023) 131496.

[13] S. Yin, L. Hua, B. Lin, N. Li, Z. Jiang, D. Dong, A mathematical model for liquid-vapor heat and mass transfer within the porous wick of loop heat pipes, Int. J. Therm. Sci. 222 (2026) 110557.

[14] S. Han, Y. Dong, G. Jin, The study on the coupled influence of water saturation on heat and mass transfer processes within porous media under CW laser irradiation, Int. J. Therm. Sci. 206 (2024) 109330.

[15] B.V. Ramarao, Moisture sorption and transport processes in paper materials, in: A. DĄBROWSKI (Ed.), Studies in Surface Science and Catalysis, Elsevier, 1999.

[16] A. Khalaf, Measuring of Thermal Conductivity and Heat Capacity of Different Papers and heat-sealing Process of Papers with a Polymer Layer, University of Maine, 2023. MS Thesis.

[17] F. Wu, M. Misra, A.K. Mohanty, Challenges and new opportunities on barrier performance of biodegradable polymers for sustainable packaging, Prog. Polym. Sci. 117 (2021) 101395.

[18] W.R. Foss, C.A. Bronkhorst, K.A. Bennett, Simultaneous heat and mass transport in paper sheets during moisture sorption from humid air, Int. J. Heat Mass Tran. 46 (2003) 2875–2886.

[19] Y.-P. Hu, W.-B. Li, S. Wu, Y.-J. Wang, W.-Z. Zhong, H. Zhang, Experimental study of the anisotropic thermal conductivity of spruce wood, Int. J. Thermophys. 44 (2023) 131.

[20] W. Wagner, A. Pruß, The IAPWS formulation 1995 for the thermodynamic properties of ordinary water substance for general and scientific use, J. Phys. Chem. Ref. Data 31 (2002) 387–535.

[21] B.V. Ramarao, S.G. Chatterjee, Moisture sorption by paper materials under varying humidity conditions, in: C.F. BAKER (Ed.), *Trans. of the Xith Fund. Res. Symp. Cambridge.* Cambridge: FRC, 1997.

[22] M.E. Parker, J.E. Bronlund, A.J. Mawson, Moisture sorption isotherms for paper and paperboard in food chain conditions, Packag. Technol. Sci. 19 (2006) 193–209.